THE JOURNAL OF PHYSICAL CHEMISTRY Letters

Letter

pubs.acs.org/JPCL

Role of the Selective Contacts in the Performance of Lead Halide Perovskite Solar Cells

Emilio J. Juarez-Perez,[†] Michael Wußler,[†,‡] Francisco Fabregat-Santiago,[†] Kerstin Lakus-Wollny,[‡] Eric Mankel,[‡] Thomas Mayer,[‡] Wolfram Jaegermann,[‡] and Ivan Mora-Sero*,[†]

[†]Photovoltaics and Optoelectronic Devices Group, Departament de Fisica, Universitat Jaume I, Av. de Vicent Sos Baynat, s/n, 12071 Castello, Spain

[‡]Institute of Materials Science, Technische Universität Darmstadt, Petersenstr. 23, D-64287 Darmstadt, Germany

Supporting Information

ABSTRACT: The effect of electron- and hole-selective contacts in the final cell performance of hybrid lead halide perovskite, $CH_3NH_3PbI_3$, solar cells has been systematically analyzed by impedance spectroscopy. Complete cells with compact TiO_2 and spiro-OMeTAD as electron- and hole-selective contacts have been compared with incomplete cells without one or both selective contacts to highlight the specific role of each contact. It has been described how selective contacts contribute to enhance the cell FF and how the hole-selective contact is mainly responsible for the high V_{oc} in this kind of device. We have determined that the recombination rate is mainly governed by the selective contacts. This fact has important implication for the future optimization of perovskite solar cells. Finally, we have developed a method to analyze the results obtained, and it has been applied for three different electron-selecting materials: TiO_2, ZnO, and CdS.

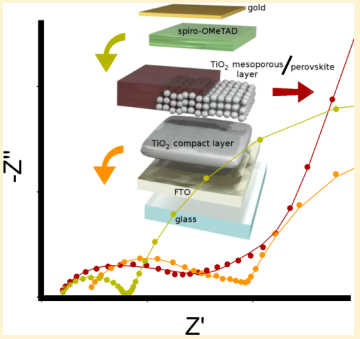

SECTION: Energy Conversion and Storage; Energy and Charge Transport

In the last few months, lead halide perovskite solar cells have experienced the fastest increase in reported efficiencies ever obtained for any photovoltaic technology. Since initial reports of all-solid lead halide perovskite solar cells with efficiencies of 10 to 11%,[1,2] a rapid succession of works has risen up the reported efficiencies to values greater than 15%.[3−5] This fast contest is leaving open many important questions about the working mechanism of this kind of solar cells. These questions should be answered to further the improvement in the performance of these photovoltaic devices. Perovskite solar cells present some differences with their most immediate predecessors, the dye-sensitized solar cells (DSCs). For example, similar efficiencies have been obtained in devices employing mesoporous TiO_2, nanostructured Al_2O_3, or even no mesoporous scaffold at all;[2,4,6] meanwhile, DSCs need a conductive and mesoporous scaffold to deposit the light harvester and collect the photocurrent. Samples with significant efficiency have been produced with no hole-transporting media.[7,8] In addition, charge accumulation in the perovskite itself has been observed, in contrast with the charge accumulation in the nanostructured TiO_2 detected in DSCs.[9] Accordingly, the physical processes occurring in these devices are not completely understood.

The photovoltaic conversions require two necessary and successive processes: carrier photogeneration and charge separation.[10] Much effort is under way to characterize the different processes occurring in the perovskite layer measuring the diffusion length in ad hoc prepared samples[11,12] or complete devices[13] or the lifetime.[14,15] But as important as the behavior of the light-absorbing material for the final device performance is the effect of selective contacts allowing an efficient charge separation.[10,16] In the case of perovskite solar cells, the most commonly used selective contact materials for electrons and holes are compact TiO_2 and spiro-OMeTAD, respectively.[17,18] Nevertheless, other materials have been found to work as selective contacts, especially for hole selectivity. Different molecules and polymers[14,19,20] and also inorganic CuI[21] have been used as hole-selective contacts. In contrast, a smaller variety of materials has been checked as an alternative electron-selective contact; C_{60},[22] graphene/TiO_2 nanocomposites,[5] and ZnO are some of the few examples.[13,23,24] Because the selective contacts play a dramatic role in the final cell performance, it is important to state clearly what their tasks are exactly. In this work, we have systematically characterized complete perovskite solar cells and incomplete cells, prepared without one or two of the selective contacts. Furthermore, we have used the results of this analysis to compare the effect of three different electron selective contacts based on TiO_2, ZnO, and CdS.

Figure 1 shows a sketch of the different layers involved in a conventional perovskite solar cell. A glass with a transparent conductive oxide layer, F-doped SnO_2 (FTO), is used as substrate. On FTO, a compact layer of TiO_2 working as selective electron contact (E) is deposited via spray pyrolysis.

Received: January 9, 2014
Accepted: January 30, 2014
Published: January 30, 2014

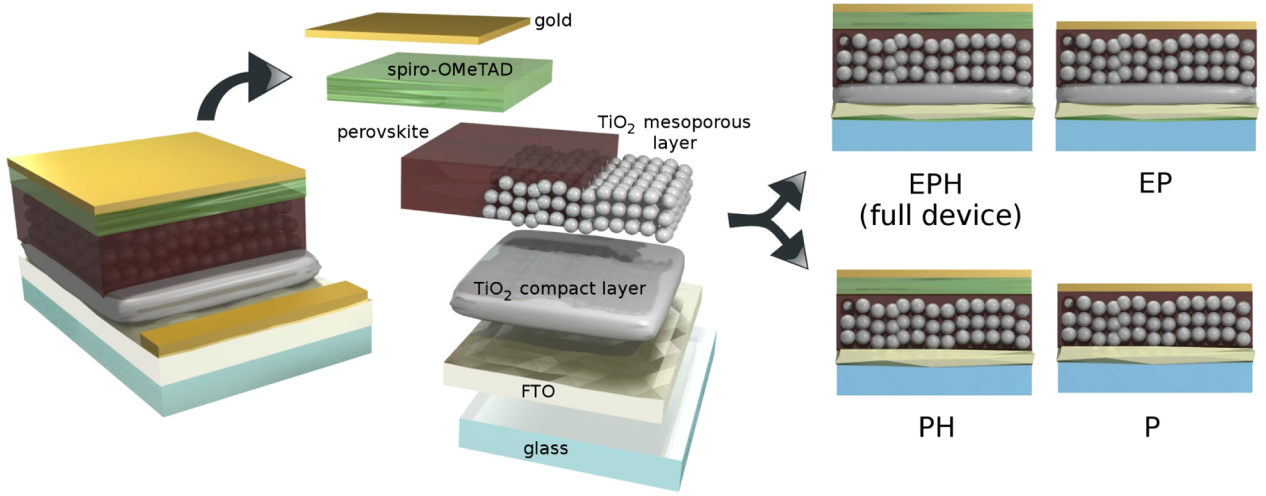

Figure 1. Configuration of the analyzed cells. The complete cell is denoted as EPH, and it is formed by an electron selective contact (E), perovskite on a mesoporous layer of TiO_2 (P), and a hole selective contact (H). Incomplete cells have been prepared without one or both selective contacts. EP samples have no hole-selective contact, just electron-selective (E) and the perovskite layer (P). PH presents no electron-selective contact; finally, the P sample is prepared without any selective contact.

The next layer is formed by thin mesoporous film of TiO_2, which is subsequently covered with perovskite (P). The perovskite used in this work has been $CH_3NH_3PbI_3$. Finally, as hole-selective contact (H) spiro-OMeTAD is spin-coated, Au electrode is subsequently evaporated. The complete device prepared in this way is denoted hereafter as EPH or complete cell. More details of solar-cell preparation can be found in the Supporting Information S1. To determine the role of the selective contact, we have prepared incomplete cells without one or two selective contacts, with the structures plotted in Figure 1. The EP sample has been prepared with an electron-selective contact but no hole-selective contact, while oppositely, the PH device has hole-selective contact but no electron selector. Finally, the P sample has a perovskite layer only, with no selective contact for either electrons or holes.

The efficiency obtained with the incomplete cells is significantly lower than the efficiency obtained for the full device; see Figure 2 and Table 1. Removing the TiO_2 layer compact, the PH sample has little effect on the open circuit potential, V_{oc}, but affects deleteriously the short circuit photocurrent, J_{sc}, and the fill factor, FF, nearly halving the photoconversion efficiency, η, in comparison with the complete device. A more dramatic effect is observed when the hole selector is removed instead of the electron selective contact,

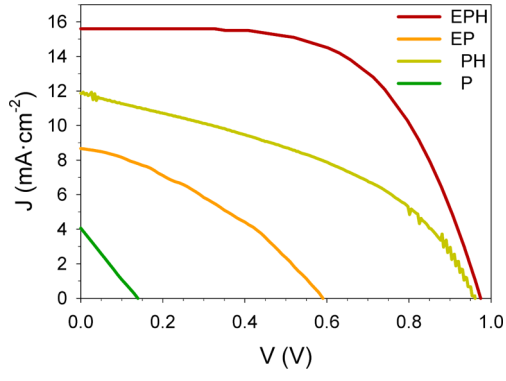

Figure 2. Current−potential $J-V$ curve of complete cell (EPH) and incomplete cells under 1 sun illumination.

Table 1. Solar-Cell Parameters of the Complete Cell (EPH) and Incomplete Cells under 1 Sun Illumination: Short Circuit Current, J_{sc}, Open-Circuit Potential, V_{oc}, Fill Factor, FF, and Photoconversion Efficiency, η, as Obtained from Figure 1[a]

cell	J_{sc} [mA/cm^2]	V_{oc} [mV]	FF [%]	η [%]
EPH	15.6	975	60.0	9.1
EP	8.6	587	35.5	1.8
PH	11.9	957	44.4	5.0
P	4.0	138	25.1	0.1

[a]See SI2 in the Supporting Information for average values and reproducibility.

sample EP, in which also V_{oc} is seriously affected. It is worth pointing out that with the proper procedures it is possible to observe significant efficiency for devices prepared with no hole-transporting media, although a low V_{oc} is a signature of these incomplete cells.[7,8] In our case, we have prepared EP sample exactly in the same way as EPH just without spiro-OMeTAD layer, and the efficiency has been seriously affected, as it has been already commented. Finally, when no selective contact at all is employed (P sample), the photovoltaic efficiency practically disappears with a reduction of two orders of magnitude with respect to the EPH sample.

To obtain a deeper insight of the role of selective contact in the performance of perovskite solar cells, we have systematically analyzed the different prepared samples by impedance spectroscopy (IS). IS has been extensively utilized for the characterization of different photovoltaic devices[25−27] and concretely all-solid DSCs and eta (extremely thin absorber)-solar cells.[28−32] IS also begins to be used in the characterization of perovskite solar cells.[9,13,24,33,34] It is a technique capable of discriminating between the different components of the device[13,26,33] and consequently able to provide abundant and useful information on the device working mechanism. We have used IS to highlight the singular and differentiated nature of perovskite solar cells by the observation of charge accumulation.[9] Here we have employed IS to characterize complete and incomplete perovskite cells of different types; see Figure 1.

dx.doi.org/10.1021/jz500059v | J. Phys. Chem. Lett. 2014, 5, 680−685

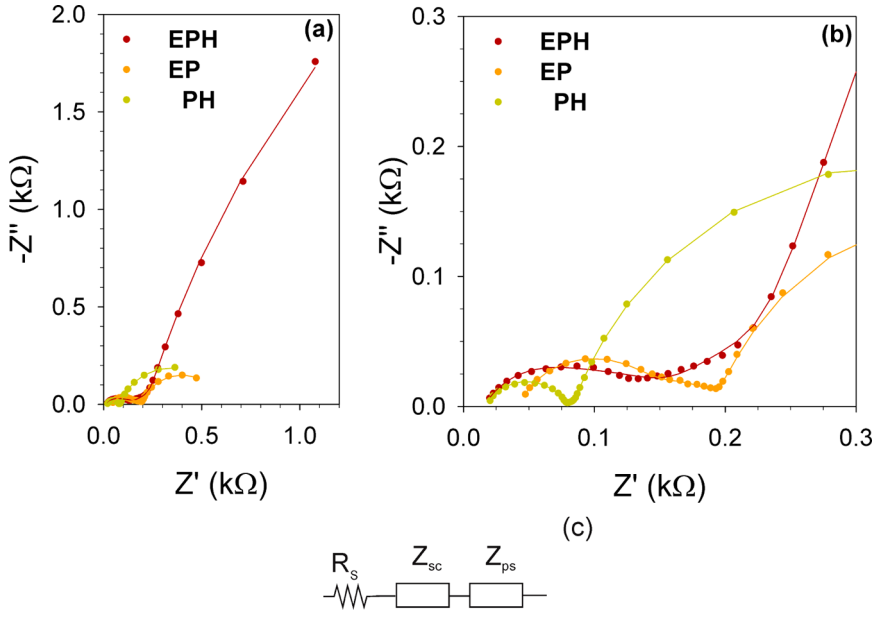

Figure 3. Nyquist plot of complete and incomplete cells at DC bias of V = 0.1 V under 1 sun illumination. (a) Complete range and (b) zoom at high-frequency region. Symbols are experimental data and solid lines correspond to the fits using the equivalent circuit in panel c. For clarity reasons, the Nyquist plot of sample P is represented in SI3 in the Supporting Information.

Cells have been analyzed under the working conditions under 1 sun illumination.

Figure 3a,b shows the Nyquist plots (imaginary vs real part of the impedance) of complete and incomplete cells at DC bias of V = 0.1 V. The impedance spectra are basically formed by two features, one at high frequency (low Z′) and the other one at low frequency (high Z′). In the simplest case, these features are just two arcs, as for the PH sample; see Figure 3b. But depending on the sample or the applied voltage, the pattern can be richer. For example, the EP sample needs two arcs to fit the low-frequency feature (see Figure 3b), while the EPH sample exhibits a transmission line (TL) pattern, with a straight line followed by an arc, for the low-frequency range feature; see Figure 3b. Consequently, different equivalent circuits have been employed to model the experimental results obtained, but in all cases the equivalent circuits present the basic elements shown in Figure 3c. A series resistance R_s is attributed to wires and FTO substrate and also additional contributions, as we show later. A Z_{sc} element is the impedance due to the selective contacts (sc) or the interface of these contacts with the perovskite layer. This contribution is responsible for the feature appearing at high frequency in the Nyquist plot.[9,13,33] To fit this part, one or two R-C circuits in series are employed, depending on if one or two merged arcs are observed in the Nyquist plot. An R-C circuit is the parallel association of a resistance, R, and a capacitor, C. However, to improve the quality of fittings, we used constant phase elements (CPE) instead of ideal capacitors. Finally, Z_{ps} is the impedance due the perovskite layer (ps). To fit this part, we have used a TL or an R-C circuit depending on whether the distinctive straight line could be recognized or not, respectively. Solid lines in Figure 3a,b represent the fitting of the experimental data using the equivalent circuit in Figure 3c.

The equivalent circuit proposed in this Letter for modeling the halide perovskite solar cell under 1 sun illumination permits us to obtain essential parameters to characterize the complete and incomplete devices. Meaningful conclusions can be drawn on the role of selective contacts for the final performance of perovskite solar cells. R_s is depicted in Figure 4a. Interestingly,

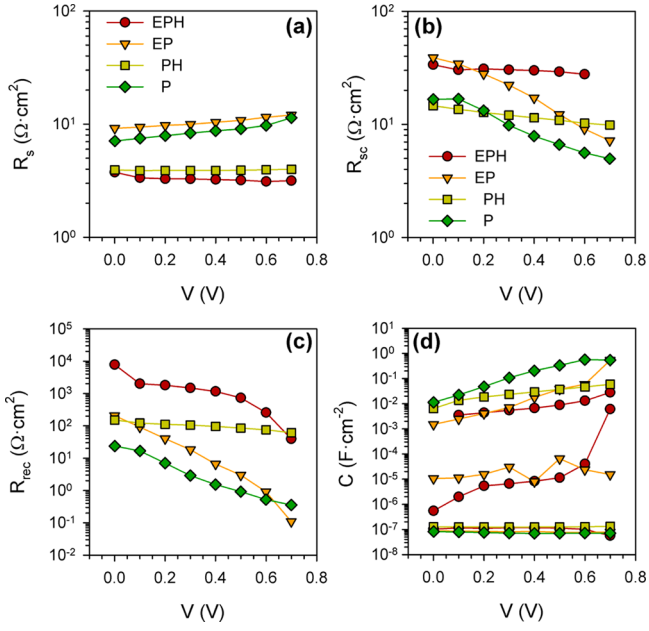

Figure 4. Parameters obtained from IS analysis of samples in Table 1. (a) Series resistance, R_s; (b) resistance of the selective contacts, R_{sc}; (c) recombination resistance, R_{rec}; and (d) capacitances obtained by IS from complete and incomplete cells. Three kinds of capacitances are observed with values ranging from 10^{-7}, 10^{-6} to 10^{-5}, and 10^{-3} to 10^{-1} F·cm^{-2}, respectively. Complete EPH cell (circles), EP (inverted triangles), PH (squares), and P (diamonds).

lower R_s is obtained for samples containing hole-selective contact, suggesting a contact resistance between perovskite and Au that disappears with the presence of spiro-OMeTAD. Consequently, one of the roles of the hole-selective contact is to reduce R_s. Series resistance plays an important role in the final device performance, as it has a deleterious effect on the FF.[35] IS allows us to determine this contributions of 4−6 Ω·cm^2 additional to the wires and FTO contributions. IS has also

dx.doi.org/10.1021/jz500059v | J. Phys. Chem. Lett. 2014, 5, 680−685

been used to detect additional contributions to R_s as a bulk contribution of silicon in Si solar cells[25] or a contribution depending on the electrolyte in DSCs.[36] In an optimization process, it is important to identify all of the possible sources of series resistance and IS is a powerful tool for this task.

R_{sc} is the resistance associated with the high-frequency feature in Nyquist plots, and it is depicted in Figure 4b. R_{sc} is obtained from the impedance Z_{sc} as just the resistance of the R-C circuit or as the sum of the two resistances when two R-Cs are employed for fitting. From Figure 4b, it can be clearly observed that the use of electron-selective layer increases R_{sc} to 15−20 Ω·cm^2. This fact is especially clear at zero voltage. R_{sc} only decreases slightly with the applied voltage for samples with selective hole conductor, while when no spiro-OMeTAD is present, R_{sc} versus V presents higher slope. This behavior indicates that when spiro-OMeTAD is used, R_{sc} is dominated by the transport resistance at the hole-selective contact.[21,28−30] However, when no spiro-OMeTAD is present, the higher slope of R_{sc} versus V indicates a charge-transfer process at the electron-selective contact interface with resistance decreasing as the voltage drop at this interface increases. R_{sc} contributes to the total series resistance, R_{series}, as $R_{series} = R_s + R_{sc}$; consequently, low values are preferable, as it has been already discussed. Thus, the use of electron-selective contacts increases R_{series} but also produces beneficial effect as the reduction of R_s or electron−hole recombination (see later).

Recombination processes are present in all photovoltaic devices, and the feature observed in the low-frequency region in the Nyquist plot of perovskite solar cells is associated with this recombination process.[13] The recombination rate is inversely proportional to the recombination resistance, R_{rec}, obtained from the fittings and represented in Figure 4c. It can be seen that in terms of absolute values the most significant effect of selective contacts is observed for R_{rec}. There are two possible explanations for this effect: the main recombination pathway is interfacial rather than bulk, at least at low applied voltages, or a bad charge extraction increases the carrier density at the bulk material and consequently the bulk recombination. The dramatic effect of selective contacts on the recombination process was previously observed by us and confirmed here with the introduction of graphene in the electron-selective contact and the enhancement observed in cell performance.[5] R_{rec} at high applied voltage significantly affects the V_{oc}.[26] Note that EPH and PH samples present the highest R_{rec} and exhibit the highest V_{oc}. The low values of R_{rec} obtained at low applied bias also negatively affect the FF because such systems behave like cell with small shunt resistance. It can be observed that the FF values and R_{rec} at low applied voltage decrease following the series EPH > PH > EP > P.

These results point out the strong influence of both selective contacts in the performance of the solar cells through FF, J_{sc}, and V_{oc}, whose behavior is particularly affected by the hole-selective contact. In fact, the highest V_{oc} reported for cells without selective hole conductor is 0.712 mV.[8] Very recently, Kamat and coworkers also observed lower R_{rec} at high applied voltages when CuI selective contact is used instead of spiro-OMeTAD, and consequently they also observed reduced V_{oc} of 0.52 V, on average, for these samples.

Figure 4d shows the capacitances obtained from the fitting of the IS data to the electrical equivalent circuits. The exact analysis of these capacitances is beyond the scope of this manuscript, but we consider it to be illustrative to represent the obtained values for other authors working in the field. Independent of the sample type, three kinds of capacitances are observed with values ranging from 10^{-7}, 10^{-6} to 10^{-5}, and 10^{-3} to 10^{-1} F·cm^{-2}, respectively. The first capacitance, 10^{-7} F·cm^{-2}, obtained at the high-frequency range exhibits lower variation with the sample type and could be associated to a geometrical capacitance. The capacitance obtained in the low-frequency range, 10^{-3} to 10^{-1} F·cm^{-2}, presents a significantly high value and could be attributed to the perovskite.[9] Finally, at intermediate values, 10^{-6} to 10^{-5} F·cm^{-2}, a third capacitance is observed but just in the case of complete and EP sample, indicating that perhaps it is related to the TiO_2−perovskite interface. In any case, further research is needed to determine unambiguously the origin of the capacitances observed in perovskite solar cells.

After the determination of the role of selective contacts in perovskite solar cell and how this effect can be analyzed by IS, we have applied this analysis to the study of three different electron selective contacts: TiO_2, ZnO, and CdS; see SI4 in the Supporting Information for work functions and band alignment cartoons. CdS is employed extensively as window and selective contact layer for electrons in CdTe, CIGS, and CZTE solar cells,[37] and as far as we know, this is the first report of its use in perovskite solar cells. Note that in the case of samples with CdS selecting contact, alumina was used instead of titania as scaffold to avoid annealing at high temperature (see SI1 in the Supporting Information), but a minor effect of the scaffold in R_{sc} has been observed.[13] Figure 5c and Table 2 show the J−V curves and the solar-cell parameters of complete cells prepared with different electron conductor materials. The lowest performance is obtained for the CdS sample that presents the lowest J_{sc} and FF but the highest V_{oc}. IS analysis is not sensitive to the photocurrent; consequently, changes in photocurrent need additional characterization techniques to be completely understood. For example, in the case of sample with CdS as electron-selective contact, CdS absorbs part of the light in the

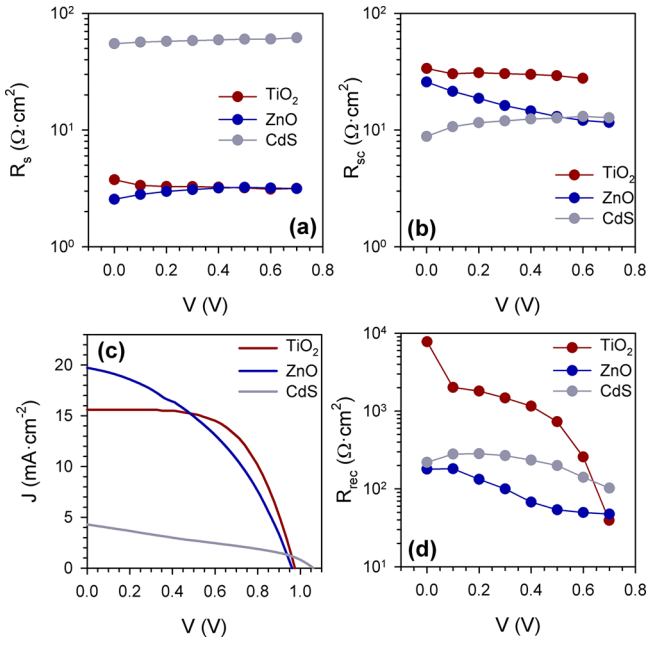

Figure 5. (a) Series resistance, R_s. (b) Resistance of the selective contacts, R_{sc}. (c) J−V curves. (d) Recombination resistance, R_{rec}, of complete cells with the electron selective contacts TiO_2, ZnO, and CdS.

dx.doi.org/10.1021/jz500059v | J. Phys. Chem. Lett. 2014, 5, 680−685

Table 2. Solar Cell Parameters of Complete Cells (EPH) under 1 sun Illumination for Different Electron Selective Contact (ESC) Materials[a]

ESC	J_{sc} [mA/cm^2]	V_{oc} [mV]	FF [%]	η [%]
TiO_2	15.60	975	60.04	9.13
ZnO	19.68	959	41.66	7.86
CdS	4.29	1058	33.84	1.53

[a]Short-circuit current, J_{sc}; open-circuit potential, V_{oc} fill factor, FF; and photoconversion efficiency, η, as obtained from Figure 1.

blue region, but these absorbed photons are not finally converted into collected electrons, as it is observed by incident photon-to-current efficiency (IPCE); see SI5 in the Supporting Information. The large J_{sc} obtained with ZnO contact is also remarkable.

From the impedance analysis, it can be observed that the CdS cell presents the highest R_{rec} at high applied voltages (see Figure 5d) and consequently the highest V_{oc}. In addition, the CdS sample exhibits the lowest FF. IS has detected that CdS-selective electron layer introduces a huge R_s more than one order higher than the one observed for TiO_2 and ZnO; see Figure 5a. The great increment in R_s cannot be compensated with a relative low R_{sc} (see Figure 5b), and finally CdS cell presents the highest R_{series} and consequently the lowest FF despite the fact that its photocurrent is sensibly lower than that for the other cells. The ZnO sample shows lower FF than TiO_2 cell. In this case, the difference in R_{series} is not very significant, but the difference in both values and slope of R_{rec}, shown in Figure 5d, is responsible for its lower FF.

In summary, the role of the selective contacts in perovskite solar cells has been investigated by IS. Both electron- and hole-selective contacts significantly affect the solar cell performance. In general, selective contacts play three major roles: transport resistance at the selector layer, charge-transfer rate at the interface (that could affect the bulk carrier density and consequently bulk recombination), and the surface recombination at the selective contact interface. It has been shown that selective contacts control the recombination resistance in perovskite solar cells. The utilization of selective contacts increments the cell series resistance, but this deleterious effect is greatly compensated for by the beneficial reduction in recombination rate. It has been observed and explained how both selective contacts contribute to enhance the cell FF, while the hole-selective contact is mainly responsible for the high V_{oc}. We have shown that IS is an appropriated method to characterize the effect of selective contacts because it allows us to discriminate the effect of the contacts in both series and recombination resistance. As an example, we have analyzed the effect of different electron selective contacts (TiO_2, ZnO, and CdS) explaining the V_{oc} and FF observed for each cell in terms of series and recombination resistances. This works shows a procedure for the characterization of selective contacts in perovskite solar cell. Because selective contacts play a dramatic role in the final device performance, its use can contribute significantly to the optimization of this kind of devices.

■ ASSOCIATED CONTENT

Supporting Information

Experimental methods, reproducibility, Nyquist plot of P sample, electron affinity, work function and band alignment, and light absorption of CdS and IPCE of CdS/perovskite sample.

This material is available free of charge via the Internet at http://pubs.acs.org.

■ AUTHOR INFORMATION

Corresponding Author

*E-mail: sero@uji.es.

Notes

The authors declare no competing financial interest.

■ ACKNOWLEDGMENTS

This work was supported by Generalitat Valenciana (ISIC/2012/008) and Universitat Jaume I project 12I361.01/1. We thank SCIC from Universitat Jaume I for the help with SEM measurements. We acknowledge Prof. Juan Bisquert for the fruitful discussion on the results shown in this manuscript.

■ REFERENCES

(1) Kim, H.-S.; Lee, C.-R.; Im, J.-H.; Lee, K.-B.; Moehl, T.; Marchioro, A.; Moon, S.-J.; Humphry-Baker, R.; Yum.; et al. Lead Iodide Perovskite Sensitized All-Solid-State Submicron Thin Film Mesoscopic Solar Cell with Efficiency Exceeding 9%. *Sci. Rep.* **2012**, *2*, 591.

(2) Lee, M. M.; Teuscher, J.; Miyasaka, T.; Murakami, T. N.; Snaith, H. J. Efficient Hybrid Solar Cells based on Meso-Superstructured Organometal Halide Perovskites. *Science* **2012**, *338*, 643−647.

(3) Burschka, J.; Pellet, N.; Moon, S.-J.; Humphry-Baker, R.; Gao, P.; Nazeeruddin, M. K.; Gratzel, M. Sequential Deposition as a Route to High-Performance Perovskite-Sensitized Solar Cells. *Nature* **2013**, *499*, 316−319.

(4) Liu, M.; Johnston, M. B.; Snaith, H. J. Efficient Planar Heterojunction Perovskite Solar Cells by Vapour Deposition. *Nature* **2013**, *501*, 395−398.

(5) Wang, J. T.-W.; Ball, J. M.; Barea, E. M.; Abate, A.; Alexander-Webber, J. A.; Huang, J.; Saliba, M.; Mora-Sero, I.; Bisquert, J.; Snaith, H. J.; et al. Low-Temperature Processed Electron Collection Layers of Graphene/TiO_2 Nanocomposites in Thin Film Perovskite Solar Cells. *Nano Lett.* **2014**, DOI: 10.1021/nl403997a.

(6) Ball, J. M.; Lee, M. M.; Hey, A.; Snaith, H. Low-Temperature Processed Mesosuperstructured to Thin-Film Perovskite Solar Cells. *Energy Environ. Sci.* **2013**, *6*, 1739−1743.

(7) Etgar, L.; Gao, P.; Xue, Z.; Peng, Q.; Chandiran, A. K.; Liu, B.; Nazeeruddin, M. K.; Gratzel, M. Mesoscopic $CH_3NH_3PbI_3/TiO_2$ Heterojunction Solar Cells. *J. Am. Chem. Soc.* **2012**, *134*, 17396−17399.

(8) Laban, W. A.; Etgar, L. Depleted Hole Conductor-Free Lead Halide Iodide Heterojunction Solar Cell. *Energy Environ. Sci.* **2013**, *6*, 3249−3253.

(9) Kim, H.-S.; Mora-Sero, I.; Gonzalez-Pedro, V.; Fabregat-Santiago, F.; Juarez-Perez, E. J.; Park, N.-G.; Bisquert, J. Mechanism of Carrier Accumulation in Perovskite Thin-Absorber Solar Cells. *Nat. Commun.* **2013**, *4*, 2242.

(10) Bisquert, J.; Cahen, D.; Hodes, G.; Rühle, S.; Zaban, A. Physical Chemical Principles of Photovoltaic Conversion with Nanoparticulate, Mesoporous Dye-Sensitized Solar Cells. *J. Phys. Chem. B* **2004**, *108*, 8106−8118.

(11) Stranks, S. D.; Eperon, G. E.; Grancini, G.; Menelaou, C.; Alcocer, M. J. P.; Leijtens, T.; Herz, L. M.; Petrozza, A.; Snaith, H. J. Electron-Hole Diffusion Lengths Exceeding 1 Micrometer in an Organometal Trihalide Perovskite Absorber. *Science* **2013**, *342*, 341−342.

(12) Xing, G.; Mathews, N.; Sun, S.; Lim, S. S.; Lam, Y. M.; Grätzel, M.; Mhaisalkar, S.; Sum, T. C. Long-Range Balanced Electron- and Hole-Transport Lengths in Organic-Inorganic $CH_3NH_3PbI_3$. *Science* **2013**, *342*, 344.

(13) Gonzalez-Pedro, V.; Juarez-Perez, E. J.; Arsyad, W. A.; Barea, E. M.; Fabregat-Santiago, F.; Mora-Sero, I.; Bisquert, J. General Working

Principles of $CH_3NH_3PbX_3$ Perovskite Solar Cells. *Nano Lett.* **2014**, DOI: 10.1021/nl404252e.
(14) Bi, D.; Yang, L.; Boschloo, G.; Hagfeldt, A.; Johansson, E. M. J. Effect Different Hole Transport Materials on Recombination in CH3NH3PbI3 Perovskite-Sensitized Mesoscopic Solar Cells. *J. Phys. Chem. Lett.* **2013**, *4*, 1532−1536.
(15) Zhao, Y.; Zhu, K. Charge Transport and Recombination in Perovskite $(CH_3NH_3)PbI_3$ Sensitized TiO_2 Solar Cells. *J. Phys. Chem. Lett.* **2013**, *4*, 2880−2884.
(16) Green, M. A. Photovoltaic Principles. *Physica E* **2002**, *14*, 11−17.
(17) Park, N.-G. Organometal Perovskite Light Absorbers Toward a 20% Efficiency Low-Cost Solid-State Mesoscopic Solar Cell. *J. Phys. Chem. Lett.* **2013**, *4*, 2423−2429.
(18) Snaith, H. J. Perovskites: The Emergence of a New Era for Low-Cost, High-Efficiency Solar Cells. *J. Phys. Chem. Lett.* **2013**, *4*, 3623−3630.
(19) Edri, E.; Kirmayer, S.; Cahen, D.; Hodes, G. High Open-Circuit Voltage Solar Cells Based on Organic−Inorganic Lead Bromide Perovskite. *J. Phys. Chem. Lett.* **2013**, *4*, 897−902.
(20) Heo, J. H.; Im, S. H.; Noh, J. H.; Mandal, T. N.; Lim, C.-S.; Chang, J. A.; Lee, Y. H.; Kim, H.-j.; Sarkar, A.; NazeeruddinMd, K.; Gratzel, M.; Seok, S. I. Efficient Inorganic-Organic Hybrid Heterojunction Solar Cells Containing Perovskite Compound and Polymeric Hole Conductors. *Nat. Photon.* **2013**, *7*, 486−491.
(21) Christians, J. A.; Fung, R. C. M.; Kamat, P. V. An Inorganic Hole Conductor for Organo-Lead Halide Perovskite Solar Cells. Improved Hole Conductivity with Copper Iodide. *J. Am. Chem. Soc.* **2014**, *136*, 758−764.
(22) Jeng, J.-Y.; Chiang, Y.-F.; Lee, M.-H.; Peng, S.-R.; Guo, T.-F.; Chen, P.; Wen, T.-C. $CH_3NH_3PbI_3$ Perovskite/Fullerene Planar-Heterojunction Hybrid Solar Cells. *Adv. Mater.* **2013**, *25*, 3727−3732.
(23) Docampo, P.; Ball, J. M.; Darwich, M.; Eperon, G. E.; Snaith, H. J. Efficient Organometal Trihalide Perovskite Planar-Heterojunction Solar Cells on Flexible Polymer Substrates. *Nat. Commun.* **2013**, *4*, 2761.
(24) Kumar, M. H.; Yantara, N.; Dharani, S.; Graetzel, M.; Mhaisalkar, S.; Boix, P. P.; Mathews, N. Flexible, Low-Temperature, Solution Processed ZnO-Based Perovskite Solid State Solar Cells. *Chem. Commun.* **2013**, *49*, 11089−11091.
(25) Mora-Seró, I.; Garcia-Belmonte, G.; Boix, P. P.; Vázquez, M. A.; Bisquert, J. Impedance Spectroscopy Characterisation of Highly Efficient Silicon Solar Cells Under Different Light Illumination Intensities. *Energy Environ. Sci.* **2009**, *2*, 678−686.
(26) Fabregat-Santiago, F.; Garcia-Belmonte, G.; Mora-Seró, I.; Bisquert, J. Characterization of Nanostructured Hybrid and Organic Solar Cells by Impedance Spectroscopy. *Phys. Chem. Chem. Phys.* **2011**, *13*, 9083−9118.
(27) Proskuryakov, Y. Y.; Durose, K.; Al Turkestani, M. K.; Mora-Seró, I.; Garcia-Belmonte, G.; Fabregat-Santiago, F.; Bisquert, J.; Barrioz, V.; Lamb, D.; Irvine, S. J. C.; et al. Impedance Spectroscopy of Thin-Film CdTe/CdS Solar Cells Under Varied Illumination. *J. Appl. Phys.* **2009**, *106*, 044507.
(28) Boix, P. P.; Larramona, G.; Jacob, A.; Delatouche, B.; Mora-Seró, I.; Bisquert, J. Hole Transport and Recombination in All-Solid Sb_2S_3-Sensitized TiO_2 Solar Cells Using CuSCN As Hole Transporter. *J. Phys. Chem. C* **2012**, *116*, 1579−1587.
(29) Boix, P. P.; Lee, Y. H.; Fabregat-Santiago, F.; Im, S. H.; Mora-Seró, I.; Bisquert, J.; Seok, S. I. From Flat to Nanostructured Photovoltaics: Balance between Thickness of the Absorber and Charge Screening in Sensitized Solar Cells. *ACS Nano* **2012**, *6*, 873−880.
(30) Mora-Seró, I.; Giménez, S.; Fabregat-Santiago, F.; Azaceta, E.; Tena-Zaera, R.; Bisquert, J. Modeling and Characterization of Extremely Thin Absorber (eta) Solar Cells Based on ZnO Nanowires. *Phys. Chem. Chem. Phys.* **2011**, *13*, 7162−7169.
(31) Fabregat-Santiago, F.; Bisquert, J.; Cevey, L.; Chen, P.; Wang, M.; Zakeeruddin, S. M.; Grätzel, M. Electron Transport and Recombination in Solid-State Dye Solar Cell with Spiro-OMeTAD as Hole Conductor. *J. Am. Chem. Soc.* **2009**, *131*, 558−562.
(32) Dualeh, A.; Moehl, T.; Nazeeruddin, M. K.; Grätzel, M. Temperature Dependence of Transport Properties of Spiro-MeOTAD as a Hole Transport Material in Solid-State Dye-Sensitized Solar Cells. *ACS Nano* **2013**, *7*, 2292−2301.
(33) Dualeh, A.; Moehl, T.; Tétreault, N.; Teuscher, J.; Gao, P.; Nazeeruddin, M. K.; Grätzel, M. Impedance Spectroscopic Analysis of Lead Iodide Perovskite-Sensitized Solid-State Solar Cells. *ACS Nano* **2014**, *8*, 362−373.
(34) Kim, H.-S.; Lee, J.-W.; Yantara, N.; Boix, P. P.; Kulkarni, S. A.; Mhaisalkar, S.; Gratzel, M.; Park, N.-G. High Efficiency Solid-State Sensitized Solar Cell-Based on Submicrometer Rutile TiO_2 Nanorod and $CH_3NH_3PbI_3$ Perovskite Sensitizer. *Nano Lett.* **2013**, *16*, 2412−2417.
(35) Sze, S. M. *Physics of Semiconductor Devices*, 2nd ed.; John Wiley and Sons: New York, 1981.
(36) Trevisan, R.; Döbbelin, M.; Boix, P. P.; Barea, E. M.; Tena-Zaera, R.; Mora-Seró, I.; Bisquert, J. PEDOT Nanotube Arrays as High Performing Counter Electrodes for Dye Sensitized Solar Cells. Study of the Interactions Among Electrolytes and Counter Electrodes. *Adv. Energy Mater.* **2011**, *1*, 781−784.
(37) Green, M. Thin-Film Solar Cells: Review of Materials, Technologies and Commercial Status. *J. Mater. Sci.: Mater. Electron.* **2007**, *18*, 15−19.